

Front-end Design Optimization for Ionoacoustic 200 MeV Protons Beam Monitoring with Sub-millimeter Precision for Hadron Therapy Applications

Elia Arturo Vallicelli^{1,2}^a, Mattia Oliver Cosmi¹, Andrea Baschiroto^{1,2}^b and
Marcello De Matteis^{1,2}^c

¹*Department of Physics, University of Milano, Bicocca, Milan, Italy*

²*Italian Institute for Nuclear Physics (INFN), Section of Milano, Bicocca, Milan, Italy*


Keywords: Nuclear Imaging, Particle Accelerator, Particle Beam Measurements, Acoustic Waves, Analog Circuits, Digital Circuits.


Abstract: This paper presents the design of a multichannel acoustic detector optimized for sensing proton induced thermo-acoustic signals (ionoacoustic signals) in clinical scenarios experiments. Ionoacoustics is a promising technique for real-time monitoring of proton beams with interesting possible applications in oncological hadron therapy. However, clinical scenarios are characterized by very low signal amplitudes (few tens millipascals). State-of-the-art experiments use general purpose acoustic sensors and heavily rely on averaging (up to thousands beam shots) to detect a clear signal, at the cost of a significant extra-dose above clinical limits. To overcome this limit, this paper presents the design of a dedicated acoustic sensor that exploits spatial correlation (multichannel sensor) to increase the SNR with no extra-dose and localize the maximum energy deposition of a 200 MeV proton beam in clinical scenarios (35 mGy/shot dose, 25 mPa signal amplitude). The results are validated by a complete cross-domain simulation of the physical (proton beam), acoustic (wave propagation) and electrical (sensor and electronics frequency response and noise) environments. The presented detector achieves a clear 20.5 dB single-shot SNR (35 mGy total dose) and can localize the maximum energy deposition with 0.5 mm precision (<1% w.r.t. the particle range) with ~1/100 dose reduction compared to state-of-the-art.


1 INTRODUCTION

Charged particles interact with matter by depositing energy along their path until they fully stop at the end of their range (Knoll, 2000). However, the energy deposition is not homogeneous, but it follows the so-called Bragg curve (shown in Fig. 1), with the highest dose deposition (defined as deposited energy per unit mass of the absorber) occurring at a certain depth within the target material corresponding to the Bragg Peak (BP). Moreover, very limited doses are deposited in the pre-Bragg and post-Bragg region. This particular feature is exploited in hadron therapy, an oncological treatment that uses beams of charged particles (mainly protons and carbon ions) to deliver high radiation doses in very specific volumes inside a

patient, corresponding to the tumor location (Parodi, 2018; Min, 2006; Hueso-González, 2018; Mirandola, 2015). This allows to damage the tumor cells while preserving the surrounding healthy tissue, with a much-localized dose deposition compared to traditional X-ray based radiation therapy. Given the high selectivity of the dose deposition, measurement techniques are required to verify during or just after the treatment that the dose has been deposited within the target volume and thus all the tumor tissue has been treated. This is usually done by means of nuclear imaging techniques (Position Emission Tomography or prompt gamma ray imaging) that however require bulky and expensive detectors and have intrinsically limited precision of new millimeters.

^a <https://orcid.org/0000-0003-0905-151X>

^b <https://orcid.org/0000-0002-8844-5754>

^c <https://orcid.org/0000-0003-1061-1262>

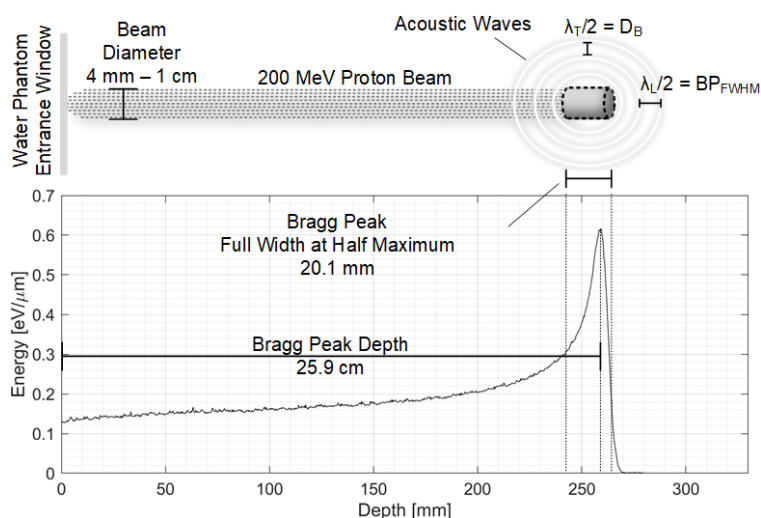


Figure 1: Bragg curve for 200 MeV Protons and ionoacoustic signal source at the Bragg Peak.

An interesting alternative Bragg Peak localization technique based on the ionoacoustic effect has been proposed by Sulak in 1979 (Sulak, 1979). The ionoacoustic effect is the generation of an acoustic wave from the fast and localized energy deposition occurring at the BP. Such acoustic wave can be acquired by a set of acoustic sensors (AS) to precisely localize the BP in space. The Time of Flight (ToF) of the acoustic wave travelling from the BP to the AS can be measured and thus the distance between the BP and the AS can be calculated, localizing the BP in space. Such technique requires a simpler detector and has proved sub-mm precision at pre-clinical and clinical energies. Hayakawa acquired a clear acoustic signal during an hepatic cancer treatment in 1995, whereas more recently sub-mm precision has been achieved using water phantoms by various experiments at clinical energies (Hayakawa, 1995; Assmann, 2015; Lehrack, 2020; Patch, 2016; Jones, 2016).

However, state of the art experiments use off-the-shelf general purpose detectors (acoustic sensors and electronics) that limit the measurement performance, as shown in (Riva, 2018; Vallicelli, 2019; Vallicelli, 2020; Samir, 1979). To improve the Signal-to-Noise Ratio (SNR), state of the art heavily relies on post-processing (in the form of averaging up to 1000 different beam shots). However, this SNR improvement comes at the cost of an extra-dose (that would be delivered to the patient in clinical applications) that exceed clinical limits, effectively preventing this technique to be applied in clinical scenarios (Vallicelli, 2020).

To overcome this limitation, this work proposes a different approach to improve the SNR without

introducing extra-dose. Instead of temporal averaging (i.e. averaging of multiple beam shots), the concept of spatial averaging is presented, in the form of averaging the signals acquired by different acoustic sensors. Multichannel acoustic sensors (MAS) are composed by N_{ch} independent acoustic sensors (channels), whose outputs are sensed simultaneously by N_{ch} different acoustic sensors. Effectively, for each beam shots, N_{ch} different signals are acquired and can be averaged to improve the SNR without any extra dose compared to a single-channel AS approach, that would require N_{ch} different beam shots (and thus N_{ch} times the dose) to achieve the same SNR increase.

Nevertheless, this multichannel approach requires a dedicated sensor and analog front-end design and cannot rely on off-the-shelf components. For this reason, this paper presents the design and characterization of a detector (called High-Energy Proton Sound Detector, HE-ProSD) that can localize the BP in space with sub-mm precision in a clinical scenario characterized by a 200 MeV proton beam delivering 10 mGy/shot dose at the BP and generating a 1 Pa acoustic signal at the BP and 23 mPa amplitude at the sensor surface, located 7.5 cm away from the BP. Such characteristics are typical of ionoacoustic experiments at clinical energies such as (Assmann, 2015) and (Jones, 2016).

This work is organized as follows. Section II presents the main characteristics of the 200 MeV experimental scenario. Section III presents the AS and AFE design that will be characterized by extensive cross-domain simulations whose results are presented in Section IV. Finally, in Section V these results will be discussed, and conclusions will be drawn.

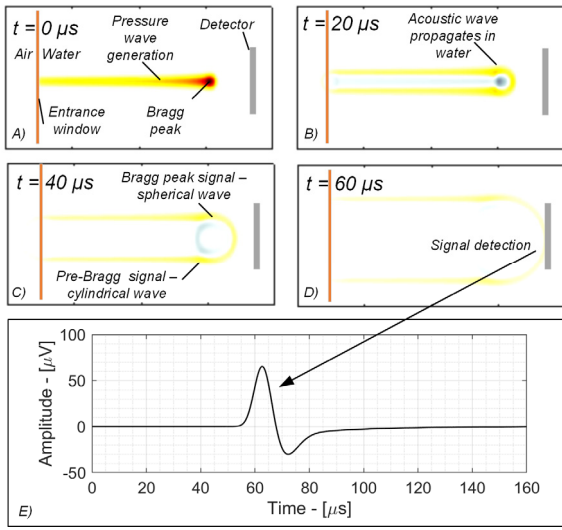


Figure 2: Ionoacoustic signal propagation and sensing.

Table 1: Characteristics of pre-clinical and clinical scenarios.

Proton Energy	20 MeV	65 MeV	200 MeV
Protons per shot	10^6	10^6	10^6
Beam range in water	4.1 mm	38 mm	259 mm
BP _{FWHM}	0.3 mm	2.9 mm	19.2 mm
Dose/shot at BP	800 mGy/shot	100 mGy/shot	35 mGy/shot
Pressure at BP	80 Pa	10 Pa	3.5 Pa
Pressure at AS	5 Pa	300 mPa	25 Pa

2 200 MeV PROTONS EXPERIMENTAL SCENARIO

Ionoacoustic experiments become more critical when the beam energy increases because the dose deposited at the BP will be increasingly lower and this results in a weaker pressure signal.

Whereas sub-clinical experiments at 20 MeV energy are characterized by tens or hundreds of Pa at the BP, this value decreases to around 5 Pa at 65 MeV (lowest energy for clinical applications) and around 1 Pa for 200 MeV (highest energy for clinical applications). A brief comparison between pre-clinical and clinical scenarios is presented in Table 1. In this work a 200 MeV proton beam scenario has been chosen because it represents the most critical scenario for ionoacoustic signal sensing and is therefore the most interesting to show the capability of the spatial averaging approach. 200 MeV protons

are characterized by a high penetration and a low dose, which gives rise to a weak and low frequency acoustic signal, two characteristics that make it difficult to use them for localization of the Bragg peak. More precisely, the BP is at 25.9 cm depth in a water phantom and the ionoacoustic signal (at 7.5 cm from the BP in the axial direction) has an amplitude of 25 mPa and a frequency spectrum that peaks at 40 kHz, as reported in (Assmann, 2015) and (Jones, 2016). Fig. 2 shows the typical ionoacoustic experimental setup. The proton beam enters in the water tank passing through a Kapton entrance window and deposits energy following the Bragg curve, that generates a correspondingly increase in pressure (acoustic source) highlighted in yellow-red in Fig. 2.A, where red indicates a higher dose and pressure, whereas yellow indicates a lower dose and pressure variation.

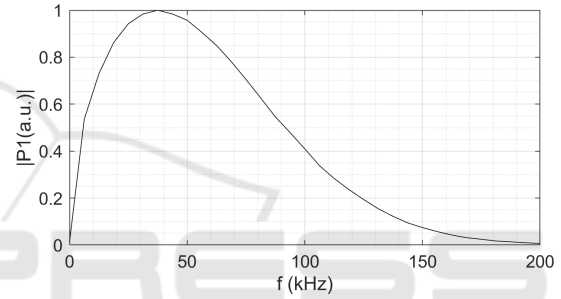


Figure 3: 200 MeV protons ionoacoustic signal spectrum.

The pressure wave propagates in water (Fig. 2.B and C shown 20 μ s and 40 μ s after the beam shot respectively) and reaches the detector surface after around 60 μ s, as shown in Fig. 2.D, where it is transduced in voltage domain, as represented in Fig. 2.E. With reference to Fig. 2.C, two different acoustic signals can be observed, one originated in the BP that propagates spherically and can be used for BP localization and one other in the pre-Bragg region, that propagates as a cylindrical wave mostly perpendicular to the beam axis.

This scenario has been completely modelled using Geant4 to estimate the energy deposition profile, k-Wave to simulate the pressure wave propagation in space (Fig. 2) and Matlab to model the AS and AFE in terms of frequency response and noise power.

The acoustic signal spectrum is shown in Fig. 3 and peaks below 40 kHz, as shown in (Assmann, 2015) and (Jones, 2016).

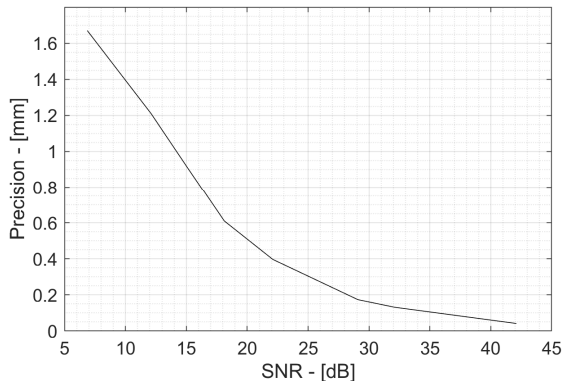


Figure 4: Precision vs SNR.

Table 2: HE-ProSD Performance Requirements.

Parameter	Value
Beam Energy	200 MeV protons
Dose/shot @ Bragg peak	35 mGy
Acoustic Signal Bandwidth	40 kHz
Signal amplitude	25 mPa _{0-peak}
Desired Precision	0.5 mm
Required HE-ProSD SNR (SNR _{HE-ProSD}) for 0.5 mm precision	20 dB
AFE Noise Figure (NF _{AFE})	1 dB
Directivity Noise Figure (NF _{DIR})	1 dB
Acoustic Sensor SNR (SNR _{AS})	22 dB

Finally, the BP-AS distance (d_{BP-AS}) can be calculated by measuring the acoustic wave time of flight (ToF) and applying equation (1), where c_w is the sound speed in water, equal to 1498 m/s at 23°C.

$$d_{BP-AS} = ToF \cdot c_w \quad (1)$$

To determine the localization precision, the distance d_{BP-AS} has been repeatedly measured 1000 times with different noise realizations. Random noise fluctuations shift the measured position in space, thus introducing a random error with a standard deviation equal to the localization precision. Repeating the measurements 1000 times (with the same SNR but different noise realization) guarantees a good statistic and an accurate measurement precision evaluation.

3 HIGH-ENERGY PROTON SOUND DETECTOR DESIGN

3.1 HE-ProSD Design Requirements

The first step in the HE-ProSD design is to define the specifications to be met. The desired localization precision has been set to 0.5 mm.

The relationship between SNR and measurement precision was obtained by measuring the precision as described in Section II, obtaining the d_{BP-AS} precision at different SNR values. The results are shown in Fig. 4. To achieve sub-mm precision a minimum 14 dB SNR is required, whereas to obtain the desired 0.5 mm precision the detector SNR needs to be as high as 20 dB. However, this SNR value has to be achieved at the detector output, including AS and AFE noise power and acoustic sensor non-idealities that will be described in the next section. For this reason, the acoustic sensor SNR (SNR_{AS}) must be larger than the final required detector SNR (SNR_{HE-ProSD}, 22 dB) because it degrades due to the analog front-end noise power and acoustic sensor BP-AS misalignments (caused by non-ideal AS directivity). These factors cause an SNR loss that require the the SNR_{AS} to be higher than the final SNR_{HE-ProSD} by an amount equal to the AFE Noise Figure (NF_{AFE}) and the AS directivity Noise Figure (NF_{DIR}), following equation (2).

$$SNR_{HE-ProSD} = SNR_{AS} - NF_{AFE} - NF_{DIR} \quad (2)$$

At this point, a NF_{AFE} and NF_{DIR} budget can be assigned to the AFE, equal to 1 dB each, thus bringing the final SNR_{AS} requirement to 22 dB. Considering a 25 mPa signal amplitude, such SNR_{AS} value corresponds to an input referred sensor noise power of 1.4 mPa_{RMS}.

Effectively, this first design step determines the performance requirements for the AS, which are listed in Table 2.

Each channel of the MAS needs to fulfill different requirements:

- The AS resonance frequency needs to match the 40 kHz signal bandwidth;
- The single-channel Output-Referred Noise Power (ORN) must be high enough so that the AFE noise requirements imposed by the 1 dB NF_{AFE} can be met;
- The single channel sensor must be able to acquire signals coming from different directions limiting their attenuation to that imposed by the NF.

The design of a single channel that meets the requirements of bandwidth, noise and directivity will be presented first. Then the number of channels necessary to obtain the required SNR_{AS} value (22 dB) through spatial averaging will be determined.

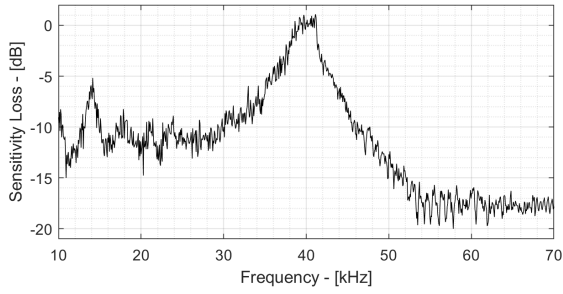


Figure 5: Acoustic Sensor frequency response.

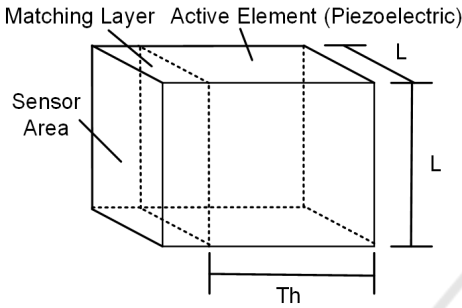


Figure 6: Single element acoustic sensor scheme.

Table 3: PIC255 PZT piezoelectric parameters.

Parameter	Symbol	Value
Frequency Coefficient	Nf	40 kHz
Relative permittivity	ϵ_0	1750
Piezoelectric voltage coefficient	g_{33}	$25 \cdot 10^{-3}$ V/(Pa·m)
Piezoelectric thickness	Th	51 mm
PIC255 Acoustic Impedance	Z_2	33 MRayl
Matching Layer acoustic impedance	Z_1	7 MRayl

3.2 Frequency Response and Sensitivity

Ionoacoustic signals are typically sensed by piezoelectric sensors that transduce pressure variations into voltage variations. Piezoelectric sensors have a frequency response characterized by a passband and a resonance frequency, as shown in Fig. 5. The sensor has its maximum sensitivity at the resonant frequency, and it decreases by about 10 dB in the linear part of the frequency response. Lead-Zirconate-Titanate are among the most performing materials commercially available for such applications.

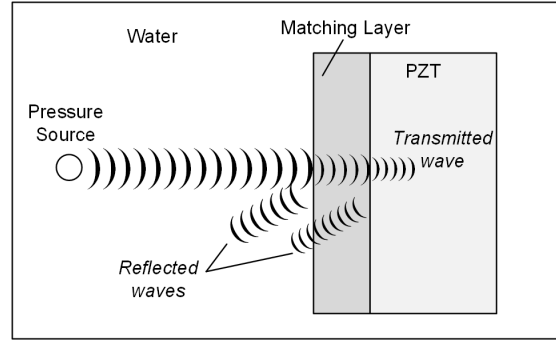


Figure 7: Acoustic impedance mismatch effects.

This section will refer to the PIC255 PZT produced by PiCeramics, whose characteristic parameters are listed in Table 3. The resonance frequency depends on the frequency coefficient N (2000 Hz·m) and on the thickness TH of the piezoelectric according to equation (n) and as shown in Figure 6.

$$f_R = \frac{N}{Th} \quad (3)$$

A resonant frequency of 40 kHz has been chosen in this case to match the signal frequency. This sets the piezoelectric thickness to 51 mm and allows to calculate the sensitivity at resonance frequency using equation (n), where g_{33} is the piezoelectric voltage coefficient, equal to 25 mV/(Pa·m):

$$S_{PZT} = g_{33} \cdot TH \quad (4)$$

Considering the 51 mm piezoelectric thickness, the PZT sensitivity is 1.3 mV/Pa. However, this sensitivity value is usually reduced to about 60-80% due to the impedance mismatch between the water (acoustic signal propagation medium) and the piezoelectric material itself (Vallicelli, 2020; Samir, 1979). In fact, whenever an acoustic wave traveling in one medium encounters another medium with different mechanical properties, it is partly transmitted and partly reflected, as shown qualitatively in Figure 7. The transmission coefficient η_T depends on the acoustic impedances of the materials (defined as the product between density and speed of sound in the medium) and is equal to:

$$\eta_T = \sqrt{\frac{2Z_2}{Z_1 + Z_2}} \quad (5)$$

Water has an acoustic impedance of 1.5 MRayl, very different from the 33 MRayl of the PZT, and therefore in a direct interface between the two materials only 40% is transmitted, causing a corresponding loss of sensitivity.

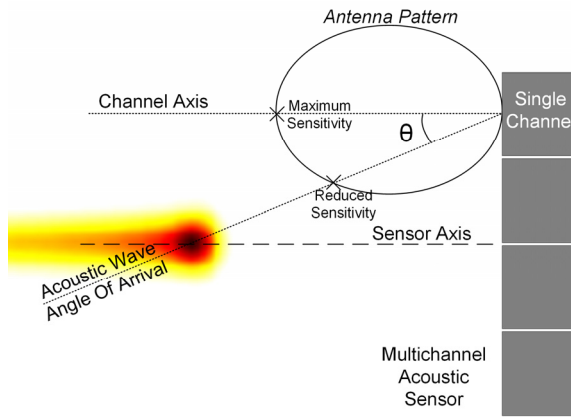


Figure 8: Sensitivity loss due to sensor directivity.

For this reason, an intermediate layer (called matching layer) is placed between the water and the piezoelectric to act as an impedance matching and increase the amplitude of the transmitted wave. A 60% transmission coefficient can be achieved with a matching material that have an acoustic impedance equal to 7 MRayl. Typical materials with 7 MRayl are silicone rubbers or araldite. Using multiple matching layers of different materials, even higher transmission coefficients can be obtained (Samir, 1979; Vallicelli, 2020). The overall sensitivity S (including piezoelectric sensitivity S_{PZT} and matching layer effects) is therefore equal to:

$$S = \eta_T \cdot g_{33} \cdot TH \quad (6)$$

The matching layer usually has a thickness equal to a quarter-wavelength to further minimize the reflected component of the acoustic wave. This leads to a final AS sensitivity of $770 \mu\text{V}/\text{Pa}$.

3.3 Sensor Capacitance and Noise Power

Piezoelectrics are capacitive sensors and thus their output referred noise power can be estimated equal to kT/C . Their capacitance, and thus output referred noise power, can be estimated from the formula for a parallel-faced capacitor, where A is the piezoelectric area, ϵ_0 and ϵ_r are respectively the dielectric constants of the vacuum (value) and relative dielectric constant of the piezoelectric material (value):

$$C = \epsilon_0 \epsilon_r \frac{A}{Th} \quad (7)$$

Thus, the output-referred noise power of the sensor channel is:

$$ORN = \sqrt{\frac{kT}{C}} = \sqrt{\frac{k T Th}{\epsilon_0 \epsilon_r A}} \quad (8)$$

Effectively, all parameters of this equation are determined except the sensor area, that can be sized to fulfill the NF_{AFE} requirement. In fact, the larger the sensor area, the smaller its ORN will be and this will force the AFE to have increasingly stringent noise specifications to meet the NF_{AFE} requirement. Ultra-low noise AFE performances ($<1 \text{ nV}/\sqrt{\text{Hz}}$ Power Spectral Density, PSD) can be reached using monolithic transistors in JFET technology (Vallicelli, 2020), which however cannot be integrated into standard CMOS technologies and therefore do not meet the miniaturization requirements needed for multi-channel sensors. On the other hand, standard CMOS processes allow high miniaturization (opening the possibility of multichannel sensor and spatial averaging) while still achieving good noise performances. An input-referred noise power spectral density of $10 \text{ nV}/\sqrt{\text{Hz}}$ was assigned to the AFE, corresponding to an integrated noise power in the signal bandwidth equal to $2.5 \mu\text{V}_{\text{RMS}}$. Such AFE IRN PSD is well within the possibilities of standard CMOS processes.

Finally, to comply with the $1 \text{ dB } NF_{AFE}$ requirements, the ORN of the MAS single channel must be equal to $5 \mu\text{V}_{\text{RMS}}$, corresponding to a 5.4 cm^2 single channel area, or a square sensor with a side length L of 2.3 cm . This sets the maximum area that fulfills the NF_{AFE} requirements.

3.4 Single Channel Directivity

Ideal acoustic sensors are omnidirectional, i.e. they can acquire a signal regardless of its direction of arrival. However, real acoustic sensors are characterized by a certain amount of directivity, that is, they attenuate signals arriving from directions other than their axis, as shown in Figure 8. This characteristic, for a given frequency of the acoustic signal, depends on the difference between the width of the acoustic sensor (L) and the wavelength. In particular, if the acoustic sensor is small compared to the wavelength it will behave almost ideally (omnidirectional), while as its size increases it will become more and more directive. Since the position of the Bragg peak is not known a priori, each channel cannot be previously oriented towards the BP.

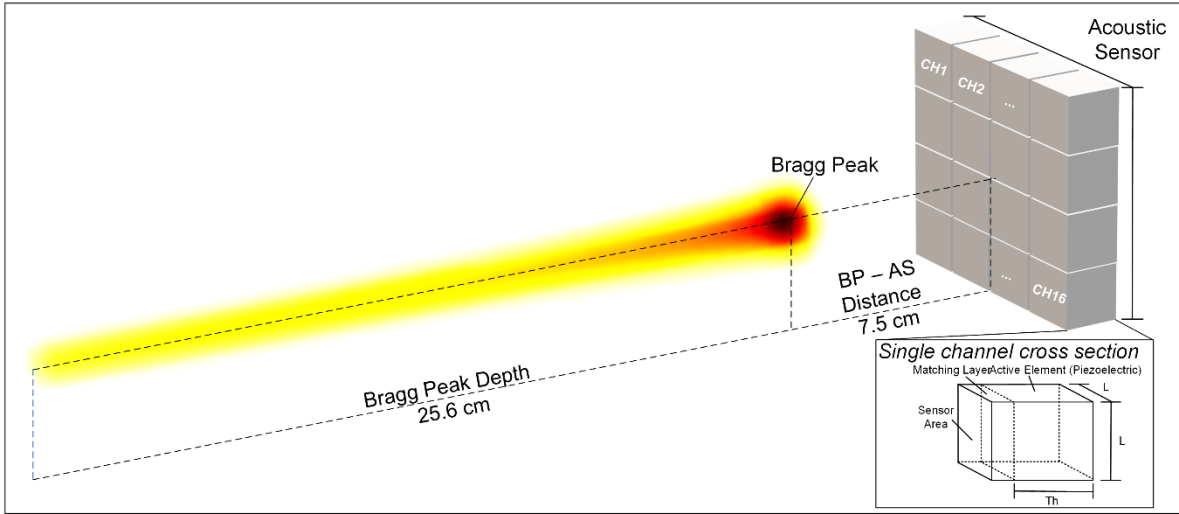


Figure 10: High-Energy Proton Sound Detector Scheme.

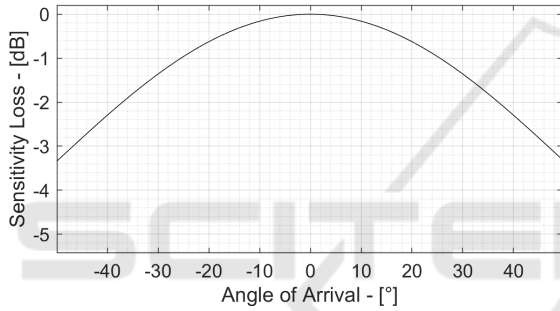


Figure 9: Single channel sensitivity loss due to its directivity.

If the single channel element is very directive, it will attenuate off-axis signals a lot, effectively lowering the AS sensitivity and final SNR. The directivity of a single channel element can be determined using the Fraunhofer laws of diffraction.

$$\frac{S(\theta)}{S} = dir(\theta) = sinc\left(\frac{\pi f L \sin(\theta)}{c_w}\right) \quad (9)$$

Considering a sensor with $L = 2.3$ cm, the overall sensitivity loss due to directivity is shown in Figure 9. In particular, considering the 7.5 cm AS-BP distance, the maximum angle to fulfil the 1 dB NF_{DIR} specification is 25° , corresponding to a 3.5 cm off-axis shift of the BP location w.r.t. the channel element. This directivity loss is particularly relevant in the case of multichannel sensors, because the presence of different channels implies that some channels are not perfectly aligned with the BP, thus

experiencing some loss due to their directivity. In this case the 2.3 cm single channel size meets the directivity requirement.

3.5 Multichannel Acoustic Sensor Design

The single channel equivalent input referred noise power can be calculated dividing the ORN by the AS sensitivity:

$$IRN_{AS} = \frac{ORN_{AS}}{S} = \frac{1}{\eta_T \cdot g_{33}} \sqrt{\frac{kT}{\epsilon_0 \epsilon_r \cdot A \cdot Th}} \quad (10)$$

Substituting the parameters found in the previous sections, the single channel capacitance is 167 pF and its input-referred noise power IRN_{AS} is equal to 6.6 mPa_{RMS}. Thus, the single channel SNR_{1Ch} is 8.5 dB. To achieve the desired 20 dB SNR, the spatial averaging technique exploits signals sensed by N_{ch} channels to improve the final SNR_{Nch} as in Equation 11.

$$SNR_{Nch} = SNR_{1Ch} + 10 \log_{10} N_{ch} \quad (11)$$

Thus, 16 channels are necessary to meet the 20 dB SNR_{AS} requirement, achieving a total 12 dB increase and a final 20.5 dB SNR_{Nch} . These channels are arranged in a 4x4 matrix to compose the HE-ProSD as shown in Figure 10.

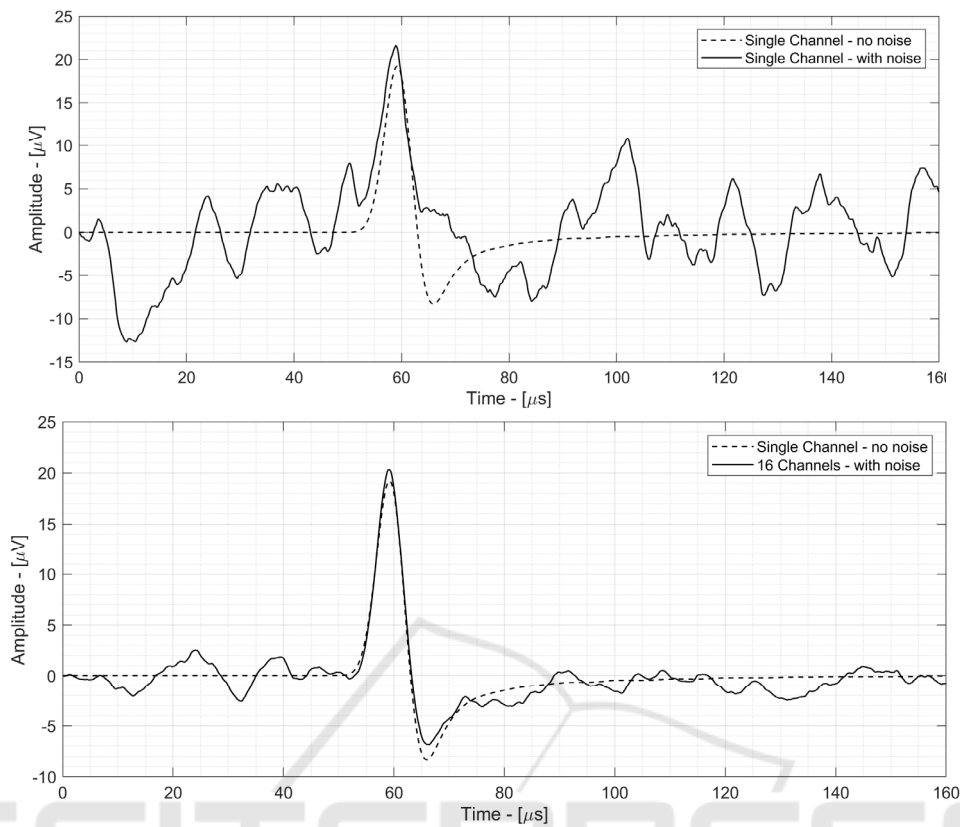


Figure 11: Top: Single channel signal including sensor and AFE noise power. Bottom: 16-channels spatial average signal including sensors and AFE noise power.

4 HE-PROSD VALIDATION AND SIMULATION RESULTS

To validate the design procedure presented in Section III and to show how a dedicated sensor can improve the localization performances, a sensor has been designed for a specific experimental scenario present in literature, represented by a 200 MeV proton beam with a 35 mGy dose deposition per shot and 7.5 cm sensor-BP distance, in a scenario equivalent to what is found in literature.

The physical environment has been simulated using Geant4 to extract the 3D dose deposition profile and thus calculate the pressure increase spatial distribution. k-Wave has then been used to simulate the pressure wave propagation in space and to determine the signal sensed by each channel of the sensor. The pressure domain signals have been transformed into voltage domain by multiplying for the sensor sensitivity of 770 μ V/Pa. Then the signal has been band-passed to represent the sensor frequency response (60 kHz -3dB frequency) and a

band-shaped thermal noise has been added. The single channel SNR ranges from 0.4 dB (central channels, closer to the BP) and 0.4 dB (external channels, further away from the BP).

Two different HE-ProSD results are presented:

- Single channel ToF measurement
- 16-channels ToF measurement

4.1 Single Channel Time of Flight Measurement

Fig. 11 shows the single-channel signal including sensor and AFE noise power, overlapped with the same signal not including noise (dotted line). The measured SNR is 8.7 dB, including sensor and AFE noise power. Although the SNR is relatively low, the ionoacoustic signal is recognizable and can be used to calculate a ToF and thus localize the BP in space. By repeating the ToF measurement with different noise realization (with the same SNR value), a 1.5 mm precision has been found.

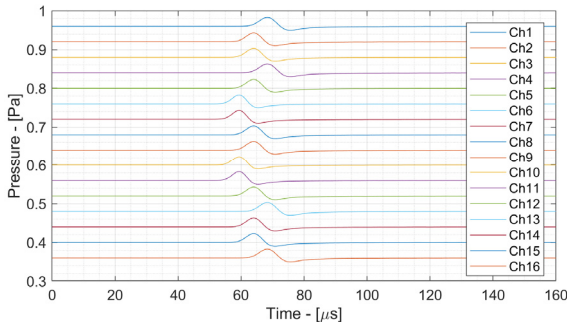


Figure 12: 16 Channels signals of HE-ProSD (without noise).

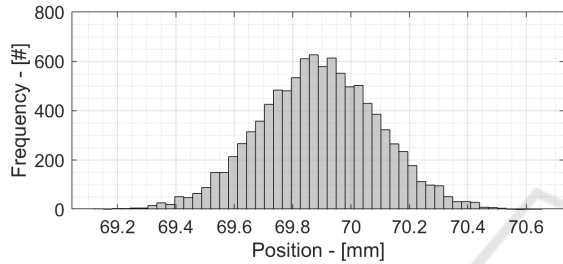


Figure 13: Measured BP position (10k repetitions) obtained by the 16-channels spatial average of the HE-ProSD.

Table 4: Comparison with state of the art.

	This work	Assmann, 2015	Jones, 2016
Proton energy	200 MeV	200 MeV	200 MeV
Acoustic Sensor	16-channels array	1 channel hydrophone	1 channel hydrophone
Acoustic Sensor Bandwidth	40 kHz	200 kHz	200 kHz
Analog Front-End	Dedicated Analog Front-End	General purpose LNA and oscilloscope	General purpose LNA and oscilloscope
Detector distance	7.5 cm	7.5 cm	5 cm
Detector noise floor	1.8 mPa _{RMS}	n.a.	27 mPa _{RMS}
Signal amplitude	25 mPa _{0-peak}	2 mPa _{0-peak}	30 mPa _{0-peak}
SNR – single shot	20.5 dB	n.a.	-2 dB
Precision – single shot	0.5 mm	n.a.	n.a.
Dose - single shot	35 mGy	n.a.	35 mGy
Final Precision	0.5 mm	0.34 mm	2.2 mm
Total Shots	1	1000	~60
Total Dose	35 mGy	10 Gy	2 Gy

4.2 HE-ProSD Time of Flight Measurement

Fig. 12 shows the 16 different signals acquired by the 16 channels of the HE-ProSD. A different offset has been applied to each channel and noise has been removed for ease of representation. Each channel signal has a slightly different phase because the distance between the acoustic source (BP) and the channels are different, and consequently the ToF. To apply the space-domain average, the 16 channels have to be re-phased. A Delay and Sum (DAS) algorithm has been applied and the output is shown in Fig. 12. Compared to Fig. 11, the SNR has improved thanks to spatial averaging, and is equal to 20.7 dB. It is important to highlight that such SNR improvement has been achieved with the same dose deposition as the single-channel SNR.

To determine the localization precision, ToF measurements have been performed with different noise realization and the resulting BP position has been shown in Fig. 14. The corresponding localization precision is 0.5 mm, obtained with a total 35 mGy dose.

4.3 HE-ProSD Performance Comparison with State of the Art

Table 4 shows a comparison between HE-ProSD performance and state of the art experiments at 200 MeV protons. Although the HE-ProSD results are obtained by simulations, all the most relevant noise and non-idealities are included and the results show a clear trend, that is that a dedicated detector design is fundamental to significantly reduce the dose necessary to achieve a given precision.

In fact, state of the art uses commercial single-channel hydrophones, general-purpose amplifiers and oscilloscopes, with the result of not optimizing SNR performance (eg integrating noise on a much higher band than that of the signal) in the digital domain and of having to compensate by resorting to averages in the digital domain. However, averaging is not an efficient tool in increasing SNR as it reduces the noise power according to $\sqrt{N_{sh}}$, thus requiring a large number of averages (and therefore extra-dose) to significantly improve SNR. Indeed, while the noise power decreases as $\sqrt{N_{sh}}$, the dose increases linearly with N_{sh} , resulting in a large extra-dose. In comparison, using the spatial mean results in an increase in SNR equal to $\sqrt{N_{ch}}$ but without using extra-dose. If the single channel of HE-ProSD were used to obtain 0.5 mm of precision using the time domain average, 16 shots of the beam would be

needed (instead of 16 channels), for a total dose of about 0.5 Gy, of the same order of magnitude. of (Assmann, 2015) and (Jones, 2016). Thanks to the dedicated design, HE-ProSD allows to obtain 0.5 mm of precision using a dose of 35 mGy, using respectively 0.35% and 1.75% dose compared to (Assmann, 2015) and (Jones, 2016).

5 DISCUSSION AND CONCLUSIONS

This paper presents the design of a multi-channel acoustic sensor that allows to locate with sub-millimeter precision a beam of protons at 200 MeV at doses compatible with those of clinical treatments. Compared to the state of the art, this detector uses a different approach, that is, it moves the SNR increase from the digital domain (post-processing) to the analog domain (detector improvement). This approach exploits a dedicated design of a multichannel acoustic sensor that allows to use the average in the space domain instead of the time domain, obtaining an increase of SNR without any extra-dose. This detector, called High-Energy Proton Sound Detector (HE-ProSD), has been validated with cross domain simulations that include 3D deposition of energy in space (Geant4), generation and propagation of the acoustic signal up to the sensor. Then, the sensor was fully modelled in mechanical (resonant frequency, physical size), acoustic (acoustic impedance and diffraction / directivity matching) and electrical (sensor capacity, input and output noise power) terms. Finally, an analog front-end was modeled in terms of frequency response and noise power and used to process the signal generated by the multi-channel acoustic sensor. To evaluate the performance of the HE-ProSD, the Bragg peak of a proton beam at 200 MeV was localized and the measurement was repeated with different noise realizations (including both acoustic sensor and electronics noise) and is An accuracy of 0.5 mm was found for an acoustic signal of 25 mPa amplitude and 35 mGy of dose deposited at the Bragg peak. By comparing these results with what has been obtained from the state of the art (Assmann, 2015; Jones, 2016), a significant dose reduction was obtained with the same localization precision. Although this work includes only simulation results and an experimental validation of the performance obtained is necessary, it is clear that for a possible application of the ionoacoustic technique in clinical scenarios it is necessary to move from off-the-shelf and general

purpose detectors to a dedicated design that exploits the potential of multichannel sensors through the development of integrated circuits front-ends to achieve high SNR in the particularly critical clinical scenarios (Baschiroto, 2009; De Matteis, 2006).

ACKNOWLEDGMENT

This work has been supported by the Proton Sound Detector (ProSD) project funded by the Italian Institute for Nuclear Physics (INFN).

REFERENCES

- Glenn F. Knoll, "Radiation Sources," in *Radiation detection and measurement*, John Wiley & Sons, 2000, ch. 1, pp. 1–28.
- Parodi, Katia, and Jerimy C. Polf. "In vivo range verification in particle therapy." *Medical physics* 45.11 (2018): e1036-e1050.
- C. H. Min, C. H. Kim, M. Y. Youn, and J. W. Kim, "Prompt gamma measurements for locating the dose falloff region in the proton therapy," *Applied Physics Letters*, Vol. 89, no. 18, pp: 1-3, November 2006.
- Hueso-González, F., Rabe, M., Ruggieri, T. A., Bortfeld, T., & Verburg, J. M. (2018). A full-scale clinical prototype for proton range verification using prompt gamma-ray spectroscopy. *Physics in Medicine & Biology*, 63(18), 185019.
- A. Mirandola, S. Molinelli, G. Vilches Freixas, et al., "Dosimetric commissioning and quality assurance of scanned ion beams at the Italian National Center for Oncological Hadrontherapy," *Radiation measurement physics*, vol. 42, no. 9, pp. 5287-5300, September. 2015.
- L. Sulak, T. Armstrong, H. Baranger, et al., "Experimental studies of the acoustic signature of proton beams traversing fluid media," *Nuclear Instruments and Methods* Vol. 161, no. 2, Pages 203-217, May 1979.
- Y. Hayakawa, J. Tada, N. Arai, et al. "Acoustic pulse generated in a patient during treatment by pulsed proton radiation beam." *Radiation Oncology Investigations* Vol. 3, no.1, pp. 42-45, Jan. 1995.
- W. Assmann, S. Kellnberger, S. Reinhardt, et al., "Ionoacoustic characterization of the proton Bragg peak with sub-millimeter accuracy," *Medical Physics*, Vol. 42, no. 2, pp. 567-574, Feb 2015.
- Lehrack, Sebastian, et al. "Ionoacoustic detection of swift heavy ions." *Nuclear Instruments and Methods in Physics Research Section A: Accelerators, Spectrometers, Detectors and Associated Equipment* 950 (2020): 162935.
- Patch, S. K., et al. "Thermoacoustic range verification using a clinical ultrasound array provides perfectly co-registered overlay of the Bragg peak onto an ultrasound

- image." *Physics in Medicine & Biology* 61.15 (2016): 5621.
- Jones, K. C., Vander Stappen, F., Sehgal, C. M., & Avery, S. (2016). Acoustic time - of - flight for proton range verification in water. *Medical physics*, 43(9), 5213-5224.
- M. Riva, E. A. Vallicelli, A. Baschirotto, and M. De Matteis, "Acoustic Analog Front End for Proton Range Detection in Hadron Therapy," *IEEE Transactions on Biomedical Circuits and Systems*, Vol. 12, no. 4, pp. 954-962, April 2018.
- Vallicelli, Elia A., et al. "Mixed-Signal Ionoacoustic Analog Front-End for Proton Range Verification with 24 μm Precision at 0.8 Gy Bragg Peak Dose." 2019 26th IEEE International Conference on Electronics, Circuits and Systems (ICECS). IEEE, 2019.
- Vallicelli, E. A., Turossi, D., Gelmi, L., Baù, A., Bertoni, R., Fulgione, W., ... & De Matteis, M. (2020). A 0.3 $\text{nV}/\sqrt{\text{Hz}}$ input-referred-noise analog front-end for radiation-induced thermo-acoustic pulses. *Integration*.
- M.A. Samir, E. Dardiry, *A Theory for Optimization in the Use of Acoustic Emission Transducers*, vol. 1, Roger Hill, 1979
- Vallicelli, Elia Arturo, et al. "22 dB Signal-to-Noise Ratio Real-Time Proton Sound Detector for Experimental Beam Range Verification." *IEEE Transactions on Circuits and Systems I: Regular Papers* (2020).
- Baschirotto, A., Delizia, P., D'Amico, S., Chironi, V., Cociolo, G., & De Matteis, M. (2009). "Low power analog design in scaled technologies". *Proceedings of the Topical Workshop on Electronics for Particle Physics, TWEPP 2009*, Pages 103-109. Paris; France; 21 September 2009
- De Matteis, M., D'Amico, S., & Baschirotto, A. (2006, June). Power-minimization design procedure for Rauch biquadratic cells. In 2006 Ph. D. Research in Microelectronics and Electronics (pp. 141-144). IEEE.